Biochemistry

pubs.acs.org/biochemistry
Article

Innate Conformational Dynamics Drive Binding Specificity in Anti-Apoptotic Proteins Mcl-1 and Bcl-2

Esther Wolf, Cristina Lento, Jinyue Pu, Bryan C. Dickinson, and Derek J. Wilson*

Cite This: *Biochemistry* 2023, 62, 1619−1630
Read Online

ABSTRACT: The structurally conserved B-cell lymphoma 2 (Bcl-2) family of protein function to promote or inhibit apoptosis through an exceedingly complex web of specific, intrafamilial protein−protein interactions. The critical role of these proteins in lymphomas and other cancers has motivated a widespread interest in understanding the molecular mechanisms that drive specificity in Bcl-2 family interactions. However, the high degree of structural similarity among Bcl-2 homologues has made it difficult to rationalize the highly specific (and often divergent) binding behavior exhibited by these proteins using conventional structural arguments. In this work, we use time-resolved hydrogen deuterium exchange mass spectrometry to explore shifts in conformational dynamics associated with binding partner engagement in the Bcl-2 family proteins Bcl-2 and Mcl-1. Using this approach combined with homology modeling, we reveal that Mcl-1 binding is driven by a large-scale shift in conformational dynamics, while Bcl-2 complexation occurs primarily through a classical charge compensation mechanism. This work has implications for understanding the evolution of internally regulated biological systems composed of structurally similar proteins and for the development of drugs targeting Bcl-2 family proteins for promotion of apoptosis in cancer.

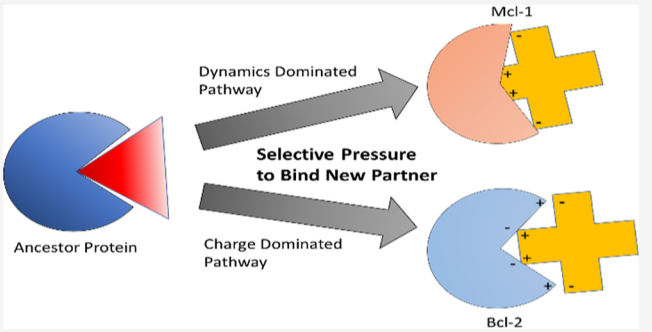

INTRODUCTION

The mitochondrial outer membrane permeabilization pathway is an essential mechanism of programmed cell death (apoptosis) and is regulated through a complex web of interactions among Bcl-2 family proteins. The Bcl-2 family encompasses many members that share Bcl-2 homology regions BH1−4: pro-apoptotic multidomain proteins (Bak and Bax), pro-apoptotic BH3-only sensitizers (Bad, Noxa, etc.), pro-apoptotic BH3-only activators (tBid, Bim, etc.), and anti-apoptotic multi-domain proteins (Bcl-2, Mcl-1, Bcl-X_L, etc.).[1]

A brief snapshot of this intricate pathway begins when truncated Bid (tBid) interacts with Bak and Bax to facilitate their oligomerization within the mitochondrial membrane.[2,3] This initiates an irreversible commitment to apoptosis as cytochrome *c* effuses from the intermembrane space, apoptosomes (Apaf-l/cytochrome *c*/caspase-9) are formed, and subsequent caspase cascades lead to cellular destruction.[4] However, anti-apoptotic proteins Bcl-2 and Mcl-1 can sequester tBid from this pathway and prevent it altogether. As such, the "dance towards death," artfully named by Kale, Osterlund, and Andrews,[1] involves exchanging pro- and anti-apoptotic partners via heterodimerization at a conserved hydrophobic BH3-binding groove.

The BH3-binding groove exists on the surface of multi-domain family members including Bak, Bax, Bcl-2, and Mcl-1. Notably, despite only sharing 33% sequence identity in their binding grooves,[5,6] anti-apoptotic members Bcl-2 and Mcl-1 have nearly superimposable 3D structures: PyMOL backbone C_α alignment of Bcl-2 (PDB 1G5M) and Mcl-1 (PDB 2MHS) for 106 core atoms yields an rmsd of 2.275 Å.[7−9] Bcl-2 and Mcl-1 strongly interact with BH3-only proteins tBid and Bim; however, at physiological concentrations, only Mcl-1 can bind Noxa and only Bcl-2 can bind Bad. This poses an intriguing question about what molecular mechanisms can enable such unique binding selectivities in such structurally similar proteins.

Mass spectrometry provides a robust toolbox for elucidating molecular mechanisms including "native" electrospray ionization mass spectrometry (ESI-MS) to observe ligand binding, complexation, and protein folding behavior; ion mobility separation mass spectrometry (IMS-MS) to analyze protein size/shape; and hydrogen-deuterium exchange (HDX-MS), covalent labeling, and cross-linking (XL-MS) to monitor structural dynamics and binding footprints with sub-molecular structural resolution.[10] In particular, "time-resolved" ESI-MS

Received: December 20, 2022
Revised: May 2, 2023
Published: May 16, 2023

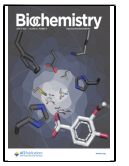

https://doi.org/10.1021/acs.biochem.2c00709
Biochemistry 2023, 62, 1619−1630

(TRESI-HDX), which uses short (ms—tens of seconds) deuterium labeling times, can characterize subtle shifts in conformational dynamics that accompany protein complexation.[11] These data can reveal binding sites and allostery and provide structural/dynamic rationales for functional properties including binding specificity.[12]

In this work, soluble Bcl-2 and Mcl-1 were examined using the mass spectrometry/hydrogen deuterium exchange toolbox to understand the molecular mechanisms that underly their distinct binding selectivities.[8,13] Ion mobility spectrometry (IMS) showed that despite being a smaller protein construct by mass, Mcl-1 (18.05 kDa) exhibited a longer drift time than Bcl-2 (20.25 kDa), agreeing with previous classical structural studies indicating that Mcl-1 has a broader binding pocket compared to other Bcl-2 family members.[9,14] Binding studies using time-resolved HDX revealed that Bcl-2 and Mcl-1 undergo distinctive shifts in their conformational ensembles that are unique to each protein and occur regardless of whether they are interacting with a partner that binds one protein or both. From this, we conclude that binding specificity in these Bcl-2 family proteins is driven not only by the charge compensation mechanisms proposed previously but also, in some cases (e.g., Mcl-1), by the ability of the ligand to induce a thermodynamically favorable shift in conformational dynamics upon complexation.

EXPERIMENTAL PROCEDURES

General. Plasmids encoding Bcl-2 and Mcl-1 were purchased from Biobasic Inc. (Toronto, Canada) and constructed based on solution stable sequences optimized by the labs of Fesik and Walensky, respectively.[8,13] Briefly, Bcl-2 was expressed in BL21(DE3) at 16 °C for 18 h using pET28a (1−34 Bcl-2, 35−50 Bcl-XL, 93−207 Bcl-2) with a C-terminal 6His tag and purified using Ni^{2+} IMAC (GE Healthcare, Fastflow). Similarly, Mcl-1 was expressed in BL21(DE3) at 16 °C for 18 h using pGEX-4T.1 encoding Mcl-1 (172−327) with an N-terminal GST-thrombin tag. GST tagged Mcl-1 was purified using GST-affinity chromatography (glutathione-sepharose resin by GE Healthcare, Fastflow). Subsequent GST-tag cleavage was carried out under rotation overnight at 4 °C (thrombin from bovine plasma, Sigma-Aldrich) followed by secondary GST-purification to remove free GST tag (untagged Mcl-1 collected in flow-through). Both Bcl-2-6His and untagged Mcl-1 were gently concentrated/buffer exchanged into a solution containing 50 mM Tris, 150 mM NaCl, and 1 mM EDTA (pH 7.0) by spin-sized centrifugal filtration (Amicon, 10 kDa MWCO) at 1200*g*, 4 °C, 12 min cycles, and resuspended by pipetting up/down between each cycle. For long-term storage at −80 °C, glycerol was added to a final concentration of 25% and the sample was aliquoted such that no tube was ever thawed more than once. Protein identity was verified by 15% SDS-PAGE and intact-MS.

BH3 Peptides. The following BH3-only peptides were synthesized and purchased from BioBasic Inc (Toronto, Canada): hBID (78−104) SQEDIIRNIARHLAQVGDSMDRSIPPG, hNOXA (19−43) AELEVECATQLRRFGDKLNFRQKLL, $hBIM_{EL}$ (141−166) DMRPEIWIAQELRRIGDEFNAYYARR, and hBAD (103−127) NLWAAQRYGRELRRMSDEFVDSFKK. For long-term storage at −80 °C, peptides were resuspended in water and aliquoted such that no tube was thawed more than once.

Native MS. 5 μM Bcl-2 or Mcl-1 was ionized by electrospray into the Waters G2-S Synapt Quadrupole-Ion Mobility Separation-Time of Flight Mass Spectrometer using a modified nanospray stage at a flow rate of 6 μL/min. To prepare for ESI-MS, the protein was buffer exchanged using Slide-A-Lyzer MINI Dialysis Devices (2 mL, 10 kDa MWCO, Thermo Scientific) into HPLC-grade 100 mM NH_4CH_3COO pH 7.

TRESI−HDX. 5 μM Bcl-2/Mcl-1, or 5 μM:30 μM Bcl-2/Mcl-1 to BH3 peptide in 100 mM NH_4CH_3COO, pH 7 (incubated on ice for 1 h), underwent rapid HDX using a time-resolved, adjustable mixer, as discussed previously.[15,16] This enabled time-resolved HDX of 1, 2, 4, and 18 s corresponding to inner-capillary pullback of 2, 5, 10, and 50 mm at protein and 100% D_2O flowrates of 2 μL/min 10% CH_3COOH was injected at 16 μL/min to maintain a constant HDX quenching pH of 2.4 after the reaction and during proteolysis. Pepsin (porcine gastric mucosa, Sigma-Aldrich) was cross-linked in-house onto NHS-activated agarose (Pierce, Thermo Fisher). The proteolytic chamber was constructed in-house using poly(methyl methacrylate) etched with a CO_2 laser (Versa-Laser) and affixed with a 0.2 μm pore-size frit upstream of the ESI emitter. Pepsin-generated peptides were identified using Proteome Discoverer 3.0 (Thermo Scientific) after LC−MS/MS analysis with the Orbitrap Elite hybrid ion trap-Orbitrap mass spectrometer. The deuterium uptake of peptides was analyzed using the G2-S Synapt (Waters) ion mobility separation mass spectrometer and processed by MS Studio.[17]

A maximal sequence coverage of 92 and 75% was obtained for Mcl-1 and Bcl-2, respectively. However, due to spectral overlap from digestion products of BH3 peptides, some sequence coverage was lost, resulting in 61% for Bcl2/Bim, 69% for Bcl2/Bid, 62% for Bcl2/Bad, 55% for Bcl2/Noxa, 84% for Mcl1/Bim, 77% Mcl1/Bad, 85% for Mcl1/Bid, and 92% for Mcl1/Noxa. Where possible, Expasy FindPept was used to identify peptides (by MS1) to make up for the loss of redundancy (e.g., 137−150 in Bcl-2/Bad).[18]

For a given data set to be accepted, Bradykinin 2−9 (PPGFSPFR, Sigma-Aldrich) was spiked in as an HDX timepoint control peptide. If Bradykinin uptake differences between the bound and unbound samples fell within the error (a statistically insignificant difference), this meant that there was no significant variation between how the two states were prepared and analyzed, and thus, any changes that did occur were accurate.

Homology Modeling with SWISS-MODEL. Homology models were constructed using the AutoModel function in SWISS-MODEL[19] of the following sequences: Bcl-2 Chimera MAHAGRTGYDNREIVMKYIHYKLSQRGYEW-DAGDDVEENRTEAPEGTESEPVVHLTLRQAGDDFSRRYRRDFAEMSSQLHLTPFTARGRFATVVEELFRDGVNWGRIVAFFEFGGVMCVESVNREMSPLVDNIALWMTEYLNRHLHTWIQDNGGWDAFVELYGPSMRHHHHHH; Mcl-1 GSGSDELYRQSLEIISRYLREQAT-GAKDTKPMGRSGATSRKALETLRRVGDGVQRNHETAFQGMLRKLDIKNEDDVKSLSRVMIHVFSDGVTNWGRIVTLISFGAFVAKHLKTINQESCIEPLAE-SITDVLVRTKRDWLVKQRGWDGFVEFFHVEDLEGG; tBid DSESQEDIIRNIARHLAQVGDSMDRSIPPGLV; Bim-(EL) AEPADMRPEIWIAQELRRIGDEFNAYYARRVFL; Bad APPNLWAAQRYGR-ELRRMSDEFVDSFKKGLP; Noxa ARAPAELEVECATQLRRFGDKLNFRQKLLNLI. The structures were analyzed using PyMol to identify protein−peptide intermolecular interactions. The quality attributes of these

https://doi.org/10.1021/acs.biochem.2c00709
Biochemistry 2023, 62, 1619−1630

Table 1. SWISS-MODEL Results and Quality

homology model	template	sequence identity (%)	global model quality estimate (GMQE)	QMEAN where 0.0 is native-like	QMEANDisCo global
Bcl-2 and Bid	PDB 4QVE	72.68	0.70	−0.67	0.70 ± 0.06
Bcl-2 and Bim	PDB 4QVF	71.91	0.68	−1.58	0.71 ± 0.07
Bcl-2 and Bad	PDB 2BZW	64.17	0.73	−1.50	0.72 ± 0.06
Mcl-1 and Noxa	PDB 2NLA	91.26	0.78	−1.65	0.79 ± 0.07

Table 2. Dissociation Coefficients Reported for Select BH3 Peptides with Bcl-2 or Mcl-1

Protein	Peptide (Start-Stop)	Sequence	Length (aa)	Bcl-2 K_D (nM)	Mcl-1 K_D (nM)
hBIM	141-166	DMRPEIWIAQELRRIGDEFNAYYARR	26	<10	<10
hBID	78-104	SQEDIIRNIARHLAQVGDSMDRSIPPG	27	50-10,000 *(20 aa)	<10 *(26 aa)
hNOXA	19-43	AELEVECATQLRRFGDKLNFRQKLL	26	>10,000	10-100
hBAD	103-127	NLWAAQRYGRELRRMSDEFVDSFKK	25	10-50	>10,000

models are listed in Table 1 and are detailed in the publication by Studer et al. (2020).[20]

RESULTS

Expression and Purification of Solution-Stable Bcl-2 and Mcl-1 Constructs. Wild-type Bcl-2 family proteins are often prone to aggregation and are difficult to express and purify, resulting in a need for truncation or loop deletion to obtain crystallographic or NMR structures. To express solution-stable recombinant Bcl-2 and Mcl-1 for this in vitro study, optimized sequences representing the Bcl-2 homology core and purification strategies published by Petros et al. (2001) and Lee et al. (2016) were used.[8,13] Petros et al. (2001) were the first to obtain a solution structure of Bcl-2. They based their solution-stable construct on Bcl-X_L, which had been the first structure solved from the Bcl-2 family in 1997.[21] By replacing the Bcl-2 ∼60 amino acid loop with the shorter loop of Bcl-X_L, they were able to reduce disorder and lower the isoelectric point of the protein from near-neutral pH to pH 5.0 while retaining its biological antiapoptotic function upon electroporation into staurosporine-treated Jurkat cells.[8]

Although attempts were made to work with purified wild-type Bcl-2 and Mcl-1, both displayed a propensity for aggregation and precipitation in MS-compatible solutions and subsequent clogging of sub-millimeter diameter capillaries used for delivery of sample to the mass spectrometer. This can be attributed to their transmembrane tails; large, disordered regions; and hydrophobic binding grooves. Consequently, all experiments discussed here use Mcl-1 (172−327) with an N-terminal SGS artifact after thrombin cleavage for GST tag removal and Bcl-2 (1−34, 35−50 Bcl-X_L, 93−207) with a C-terminal His tag. The sequences used can be found in Table S1 in addition to a split RNA-polymerase luciferase assay testing Bcl-2 and Mcl-1 Bid/Noxa binding activity compared to chimeric Bcl-2 and truncated Mcl-1 in Figure S1.[22,23]

Native Mass Spectrometry Demonstrates the Expected Binding Specificities for Bcl-2 and Mcl-1 Constructs. Previously, a review by Kale, Osterlund, and Andrews (2018) compiled over 30 publications, which reported on the binding affinities of Bcl-2 family members using various biological assays including isothermal titration calorimetry, surface plasmon resonance, and fluorescence polarization.[1,8,24−37] Table 2 is adapted from their work and lists the Bcl-2 and Mcl-1 dissociation constants (K_D) with BH3-only peptides Bim, Bid, Bad, and Noxa. Based on these measurements, Bcl-2 was expected to interact with Bid (50−10,000 nM K_D), Bad (10−50 nM K_D), and Bim (<10 nM K_D), whereas Mcl-1 was expected to interact with Bid (<10 nM K_D), Bim (<10 nM K_D), and Noxa (10−100 nM K_D). To confirm this and obtain the optimal molarity ratio of protein and BH3 peptide for the saturated "bound" protein state, native ESI-MS was used.

Native mass spectra are shown in Figure 1, starting with the unbound Bcl-2 and Mcl-1 spectra in panels A and B, respectively. Both proteins exhibited a similar, narrow charge distribution dominated by the 9+ and 8+ charged state and minimally populated by 10+ and 7+. For Bcl-2, the four m/z charge peaks correspond to 2013.19, 2236.84, 2516.24, and 2875.60, whereas for Mcl-1, the four peaks correspond to m/z of 1806.41, 2006.93, 2257.64, and 2579.86. Using ESIprot deconvolution, the average masses of Bcl-2 and Mcl-1 were calculated to be 20,121.69 ± 0.85 and 18,051.88 ± 1.04 Da, respectively (Figure 2).[38] Although Mcl-1 matched its theoretical mass (18,053.47 Da) based on its primary sequence, Bcl-2 (20,253.53 Da) was off by −131.84 Da, which could be attributed to N-terminal methionine loss, a hypothesis supported by the N-terminal peptide later observed in HDX-MS experiments (shown in Figure 3, peptide 2−13).

Next, 5 μM Bcl-2 or Mcl-1 was incubated with each BH3 peptide at a 1:1, 1:2, 1:4, and 1:6 molar ratio. As shown in Figure 1C−H, a ratio of 1:6 generated saturated "bound" native spectra for known interactors, and this was used as the optimal ratio for all subsequent HDX experiments (Figure 2). Dotted lines from Figure 1A,B indicate the unbound peaks for Bcl-2 and Mcl-1. For Bcl-2 + Bim (23,392.68 Da), the bound m/z peaks correspond to 2340.27 (10+) and 2600.20 (9+); for Bcl-2 + Bad (23,226.26 Da), the bound m/z peaks correspond to 2323.60 (10+) and 2581.74 (9+); and for Bcl-2 + Bid (23,098.53 Da), the bound m/z peaks correspond to 2310.87 (10+) and 2567.50 (9+). The experimental masses of the complexes fell within 2.6 Da of the expected masses of 23,391.38, 23,225.20, and 23,096.01 Da, respectively. On the other hand, for the Mcl-1 + Bim complex (21,324.35 Da), the m/z peaks correspond to 2133.45 (10+) and 2370.37 (9+); for Mcl-1 + Bid (21,029.79 Da), the bound m/z peaks correspond to 2103.96 (10+) and 2337.68 (9+); and for Mcl-1 + Noxa (21,033.33 Da), the bound peaks correspond to 2104.39 (10+) and 2337.99 (9+).

Interestingly, in the Bcl-2 "bound" spectra, peaks corresponding to the complex are dominant, whereas in the Mcl-1

https://doi.org/10.1021/acs.biochem.2c00709
Biochemistry 2023, 62, 1619−1630

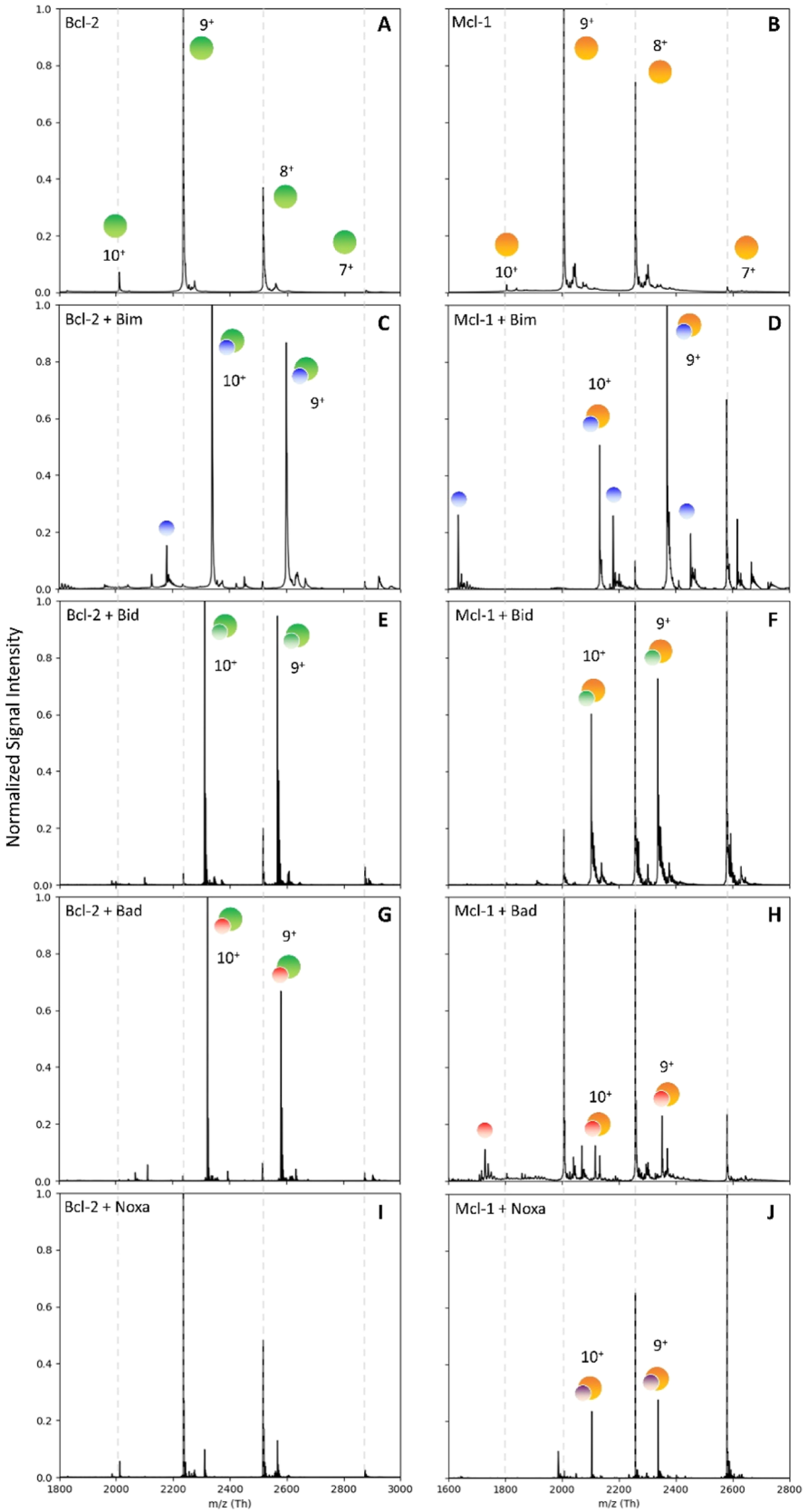

Figure 1. Native mass spectra of Bcl-2 and Mcl-1 bound to BH3 peptides: (A) Bcl-2, (B) Mcl-1, (C) Bcl-2 + Bim, (D) Mcl-1 + Bim, (E) Bcl-2 + Bid, (F) Mcl-1 + Bid, (G) Bcl-2 + Bad, (H) Mcl-1 + Noxa, (I) Bcl-2 + Noxa, and (J) Mcl-1 + Bad. Dotted lines track the position of the unbound peak in all mass spectra. The protein concentration was 5 μM and, where applicable, the peptide concentration was 30 μM.

https://doi.org/10.1021/acs.biochem.2c00709
Biochemistry 2023, 62, 1619−1630

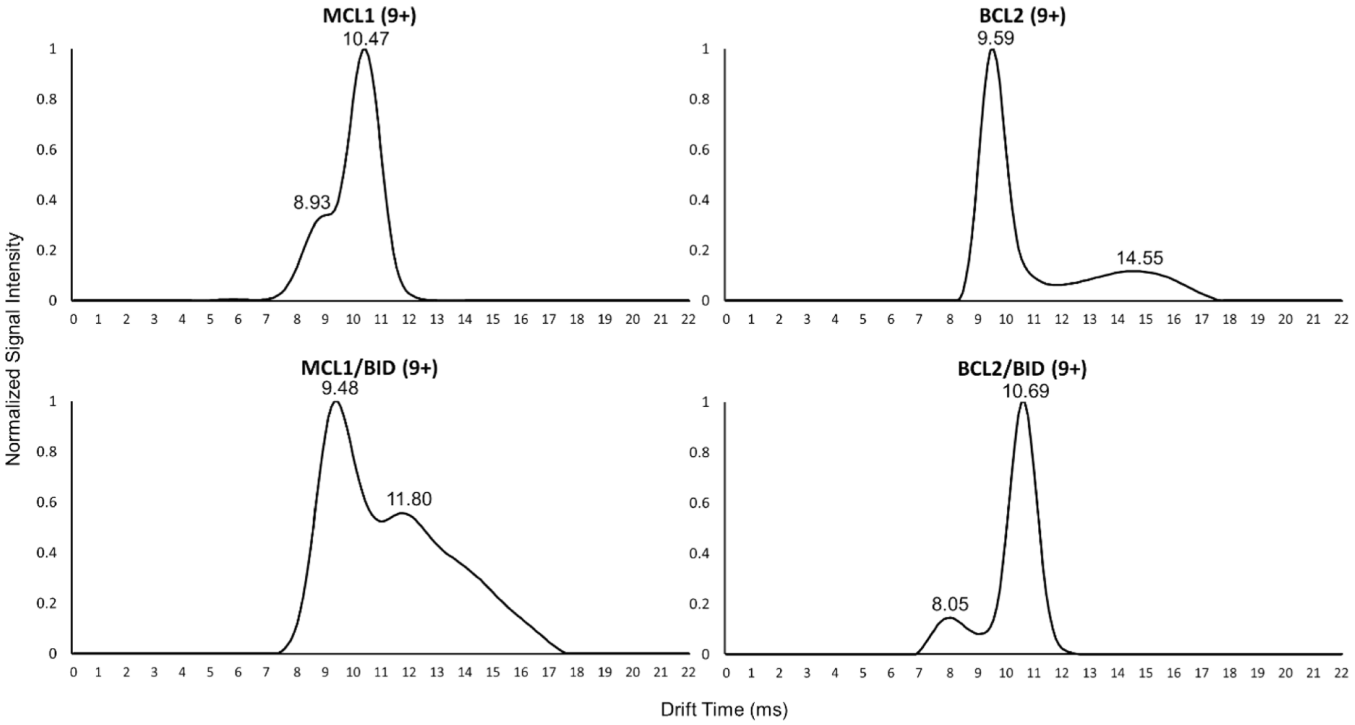

Figure 2. Ion mobility chromatograms of bound and unbound Bcl-2 and Mcl-1. The relative signal intensity as a function of drift time (milliseconds) for Mcl-1 (top left), Bcl-2 (top right), Mcl-1/Bid (bottom left), and Bcl-2/Bid (bottom right) is shown for their 9+ charge state.

spectra, binding appears to induce a shift to lower charge, even for m/z peaks corresponding to the unbound protein. This may arise from loss of Mcl-1/BH3 peptide complexes in the gas phase, accompanied by charge stripping by the departing peptide, resulting in a significant fraction of the lower-charge "unbound" peak intensity being attributable to protein that was originally "bound"' in solution.[39,40]

No interaction was detected for Bcl-2 + Noxa (Figure 1I), which is consistent with what is known about Bcl-2 specificity (Noxa is an Mcl-1-specific binder). Minor peaks corresponding to Mcl-1 + Bad (a Bcl-2 specific binder) were observed (Figure 1J), suggesting the possibility of weak binding. However, Bad did not induce the charge reduction effect observed for all other binders of Mcl-1, indicating that the maximum "bound" fraction can be estimated, based on the intensities of the "bound" peaks relative to the unbound peaks, to be no more than 25%. Note that this estimate excludes the very real possibility that some or all of the observed "bound" peaks arise from non-specific complexation or adduction, which is a common phenomenon in ESI-MS.[41]

Ion Mobility Mass Spectrometry Reveals Divergent Binding Modes of Mcl-1 and Bcl-2 in Binding the Bid BH3 Peptide. IMS-MS was used to examine the gas phase conformations that populated the native ESI-MS spectra of Bcl-2 and Mcl-1. In Figure 2, the normalized intensity of signal (ion count) is recorded as a function of the ion mobility drift time in milliseconds, with lower drift times corresponding generally to smaller globular size (via the collisional cross section) for a given charge state. The 9+ charge state was selected because it is well populated in both the unbound and bound state spectra for both proteins (and comparing structures of the same charge reduces the complexity of interpreting IMS data).

The dominant drift time peak for unbound Mcl-1 was centered on 10.47 ms, whereas the dominant peak for Bcl-2 was 9.59 ms (Figure 2, top row). This is the opposite of what might be expected intuitively, since the Bcl-2 construct used in this study is 15 residues longer—and thus somewhat larger—than the Mcl-1 construct. However, the impact of this additional sequence on the collisional cross section could easily be subsumed by differences in how the protein is packed overall. In any event, based on the dominant mobility peaks, it appears that Mcl-1 has a somewhat larger cross section than Bcl-2. It is also worth mentioning that a larger peak width is typically linked to variability of structure (cross section) in the gas phase, and the broader larger dominant peak width of Mcl-1 (fwhm of 2.07 ms) is suggestive of higher conformational heterogeneity compared to Bcl-2 (fwhm of 1.10 ms). Both proteins also exhibit minor gas phase configurations in the unbound state, suggesting a "compact" structure in the case of Mcl-1 (shoulder at 8.93 ms) and an "extended/disordered" structure for Bcl-2 (broad low peak at 14.55 ms). Additional IMS plots for the 10+ charge state can be found in Figure S2; however, the 8+ charge state was not present in bound samples (see Figure 1) and could, therefore, not be used for bound/unbound comparisons.

Upon complexation with the Bid BH3 peptide, Mcl-1 and Bcl-2 undergo distinct changes in their gas phase configurations. For relatively small proteins like Mcl-1 and Bcl-2, complexation with a large peptide such as Bid BH3 (2976.32 Da) could cause an increase or decrease in the ion mobility, depending on how the incoming peptide packs on to the structure and the extent to which the conformation "tightens" as new inter- and intra-molecular bonds are formed. In this case, complexation appears to have had the opposite effects on Mcl-1 and Bcl-2 drift times, resulting in a "tightening" of the structure for Mcl-1 (10.47 ms → 9.48 ms) and a larger cross section for Bcl-2 (9.59 ms → 10.59 ms). At the same time, the minor peaks have switched places relative to the main peaks, so that bound Mcl-1 is exhibiting a new extended configuration

https://doi.org/10.1021/acs.biochem.2c00709
Biochemistry 2023, 62, 1619−1630

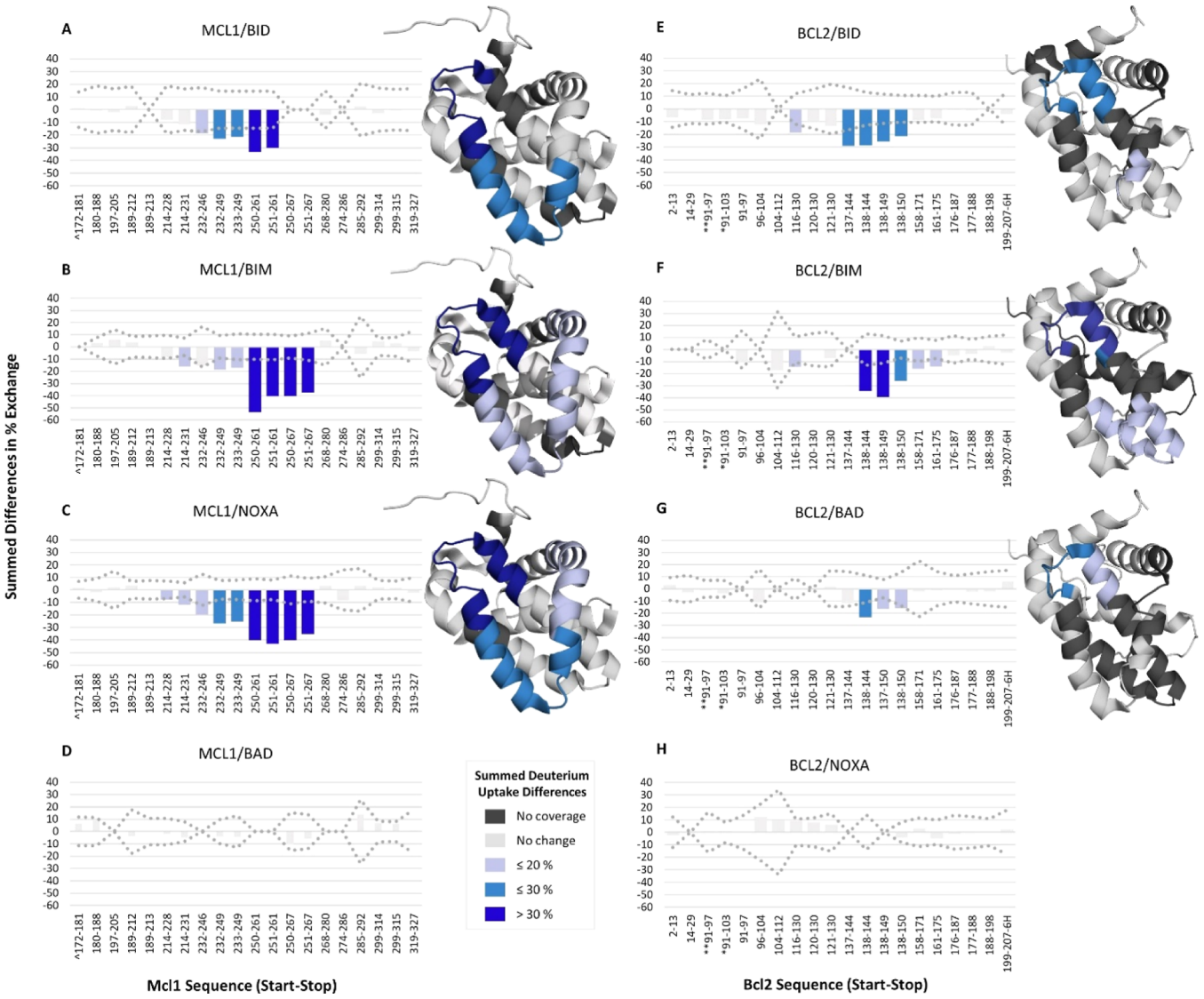

Figure 3. Difference in % deuterium exchange of complexed versus unbound Bcl-2 and Mcl-1. HDX difference plots comparing deuterium uptake in Mcl-1 and Bcl-2 in the presence and absence of BH3 peptides from (A,E) Bid, (B,F) Bim, (C,H) Noxa, and (D,G) Bad. The differences in magnitudes are obtained by subtracting raw uptake values from the kinetic plots shown in Figures S7−S14. Colored bars indicate statistically significant decreases in uptake upon complexation with the significance threshold for each peptide (difference magnitude > 2σ, $n = 6$), represented by the dotted line. To the right of each plot, HDX difference magnitudes are mapped onto the corresponding PDB structures.

(11.80 ms) and Bcl-2 is exhibiting a new compact state (8.05 ms) upon binding. Additional IMS chromatograms of Bcl-2 and Mcl-1 complexed with BH3 peptides can be found in Figure S3 and are consistent with the dominant drift time peaks observed in BID-bound mobiligrams. IMS of Bcl2/Noxa and Mcl1/Bad were compared to protein-only spectra, shown in Figures S4 and S5, as a negative control.

Taken together, these IMS data suggest significantly different binding modes for Mcl-1 and Bcl-2 in their interaction with Bid; however, any characterization of these differences from IMS alone would be, at best, highly speculative, and there is no guarantee that these gas phase observations directly reflect the process in solution. Our next step was, therefore, to undertake a TRESI-HDX analysis, which reflects structure and conformational dynamics in solution.

Time-Resolved HDX-MS Shows Dynamics-Driven Complexation Uniquely in Mcl-1, Regardless of the Binding Partner.

To explore whether the IMS observations were consistent with global structure and conformational dynamics in solution, we first carried out "global" hydrogen deuterium exchange measurements for the intact proteins (Figure S6). These data agree with the broad conclusions drawn from the IMS measurements, specifically that Mcl-1 is more dynamic in the unbound state than Bcl-2; however, to examine this system with sufficient spatial resolution to draw specific conclusions about the binding mechanism, we require segment-level data of the type provided by the "bottom−up" TRESI-HDX workflow.

The TRESI-HDX method for bottom−up millisecond hydrogen deuterium exchange has been described previously.[11,15,16] This approach enables "segment-averaged" (peptide-level) measurements of deuterium uptake with millisecond−second labeling times, which can probe subtle shifts in conformational dynamics resulting from complexation. In Figure 3, the local TRESI-HDX data are presented

https://doi.org/10.1021/acs.biochem.2c00709
Biochemistry 2023, 62, 1619−1630

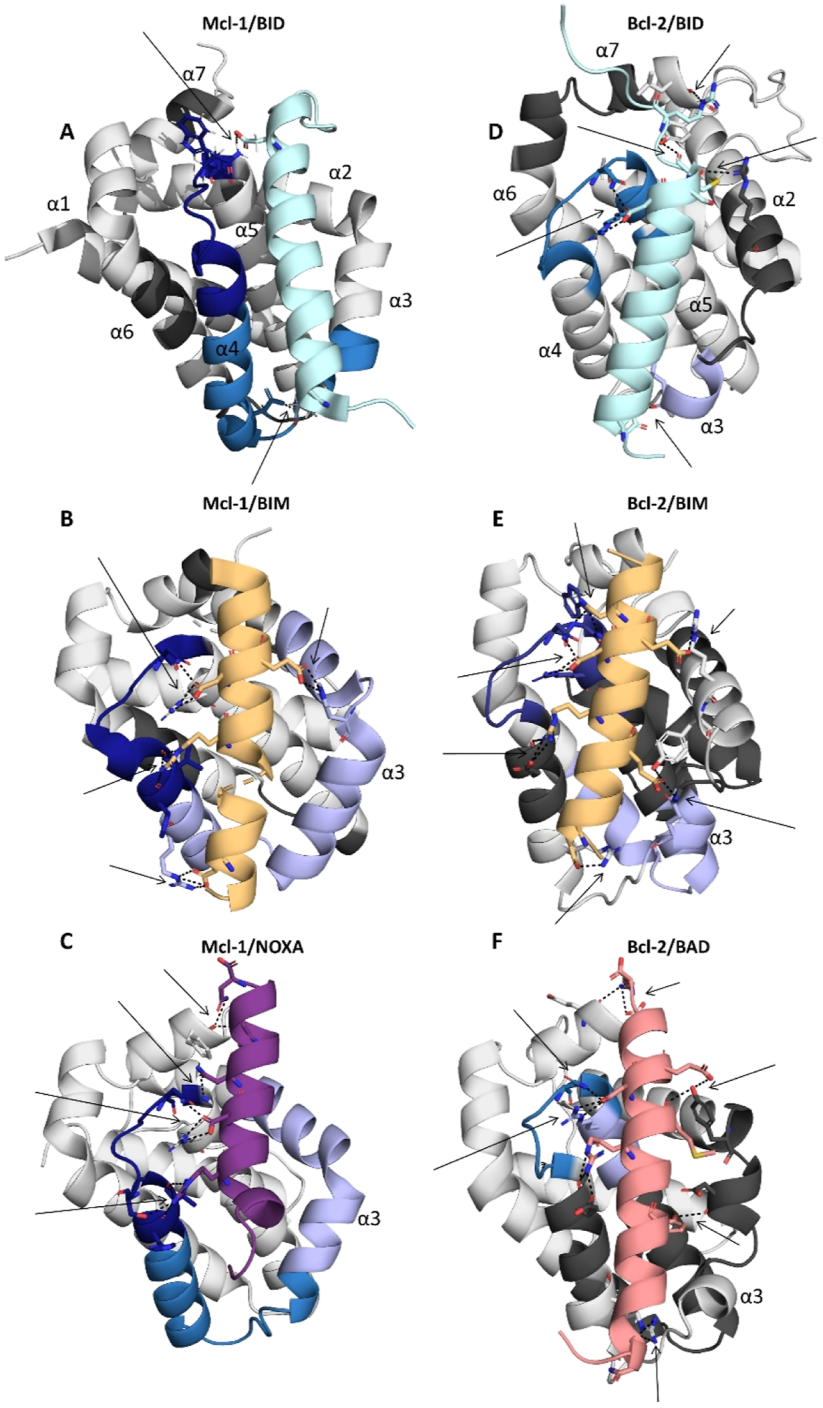

Figure 4. Homology models and PDB structures displaying intermolecular bonding. Intermolecular bonds are denoted in black dashed lines and emphasized with black arrows. Mcl-1 is on the left (A−C), and Bcl-2 is on the right (D−F). For the BH3 peptides, Bid is shown in cyan, Bim is shown in yellow, Bad is shown in salmon, and Noxa is shown in violet. The structures are colored based on the summed HDX differences from Figure 3: no sequence coverage (black), no change (light grey), ≤20% (light blue), ≤30% (sky blue), and >30% (royal blue).

differentially, meaning that deuterium uptake in unbound protein is subtracted from uptake in the peptide-bound protein, and then the differences at each timepoint were summed. As a result, bars with negative values indicate that deuterium uptake has decreased in the corresponding region because of complexation. HDX difference profiles were acquired for Bcl-2 and Mcl-1 upon complexation with peptides corresponding to the BH3 peptides of Bim, Bid, Bad, and Noxa. The raw deuterium uptake kinetic profiles that are subtracted to yield these bar plots are provided in Figures S7−S14.

One of the disadvantages of online TRESI-HDX is that without liquid chromatographic separation, it often provides lower sequence coverage than the corresponding conventional timescale experiment. Sequence coverage varied considerably depending on the system in question; the highest coverage corresponded to Mcl-1/Noxa (92%), and the lowest coverage corresponded to Bcl-2/Noxa (55%), with an average of 73% across the eight difference plots (sequence coverage and

https://doi.org/10.1021/acs.biochem.2c00709
Biochemistry 2023, 62, 1619−1630

redundancy data are provided in Table S2, and the peptide list for each protein is provided in Tables S3 and S4). Peptides in Bcl-2 involving the chimeric sequence are indicated using an asterisk (*) to denote 39−50 of Bcl-X_L or a double asterisk (**) to denote 36−50 of Bcl-X_L. In Mcl-1, the N-terminal peptide contains a thrombin cleavage site artifact (an extra S) denoted by a circumflex (^). In every case, peptides located within the binding grooves of Bcl-2 and Mcl-1 were observed.

Time-resolved HDX was used to measure the differences in deuterium uptake between Mcl-1 and Bcl-2 in the presence and absence of BH3 peptides, shown in Figure 3. The x-axes for these plots include all peptides detected for the corresponding protein. The dashed line represents the propagated error and using two-fold standard deviation (2σ) of two repeats of three technical replicates per state ($n = 6$). Bars that did not exceed this magnitude by more than 1% on the "difference in % exchange" scale are colored light gray to indicate that they were not considered statistically significant. Regions with significant changes in deuterium uptake are mapped onto NMR-derived structures of Mcl-1 (PDB 2MHS) and Bcl-2 (PDB 1G5M).[8,9] Light-, sky-, and royal blue were used to illustrate the summed differences of ≤20, ≤30, and >30%, respectively. Regions for which no peptides were obtained are denoted in black, and regions for which there was no significant change are represented in gray.

For Mcl-1/Noxa, large magnitude decreases in deuterium uptake (compared to the unbound state) were observed in peptides spanning 232−267 and late-appearing (statistically significant after 4 s) decreases were observed from 214 to 246. A nearly identical profile was observed for Mcl-1/Bim, as shown in Figure 3B. The Mcl-1/Bid profile (Figure 3A) also showed substantial decreases at 250−261 and late decreases at 232−249; however, some peptides corresponding to the 250−267 region could not be analyzed due to extensive signal overlap in the raw uptake data (see Figure S15 for an example of raw mass spectra for protected peptide 250−261). For all three interactions with Mcl-1 (i.e., Noxa, Bid, and Bim), all significant changes occurred across the conserved binding groove at helices α3−α5. In the case of Mcl-1/Bad (Figure 3D), essentially no significant changes in deuterium uptake were observed across the entire protein, consistent with the expected lack of interaction.

For Bcl-2, the interaction with Bid resulted in changes in a much narrower region corresponding to residues 137−150 (Figure 3E), which maps to an area within the Bcl-2 binding groove (see Figure S15 for an example of raw mass spectra for protected peptide 137−144). A weak signal is observed in the 116−130 region but is not observed in broadly overlapping peptides 120−130 and 121−130. The signal is, therefore, only mapped from 116 to 119 in the corresponding NMR structure. Similarly, for Bcl-2/Bim (Figure 3F), uptake decreases were observed at 138−150 together with a weak, inconsistent signal at 116−130, and a slowly developing decrease was observed in the 158−175 region. The Bcl-2/Bad complex shown in Figure 3G exhibited the weakest decreases in uptake, but these were persistent over all timepoints and occurred in the 138−150 region, in agreement with the other Bcl-2 complexes. Notably, in all three binding scenarios, the persistent decreases occurred at a localized region within the binding groove at the junction of helices α4−α5, corresponding to the BH1 domain that facilitates complexation in Bcl-2 and Mcl-1 via a conserved intermolecular salt-bridge. Bcl-2 did not exhibit any significant changes in deuterium uptake in the presence of Noxa (Figure 3H), which is consistent with the expected lack of interaction.

Static Structure-Based Homology Modeling Provides an Incomplete Picture of Complexation that can be Complemented with Dynamics Information from HDX. To further explore the chemical interactions between the human BH3 peptides and Bcl-2 or Mcl-1, we used SWISS-MODEL,[19] an open-access protein homology-modeling software package, to visualize 3D structures of Bcl-2 or Mcl-1 with "bound" BH3 peptides for which there are currently no co-crystal or NMR structures (Figure 4). In Bcl-2 homology modeling, Bcl-X_L was used as the template whereas the Mcl-1 Noxa model was based on a template of Mcl-1 bound to mouse NoxaB.

Overall, Bcl-2 was observed to form a higher number of protein−peptide interactions (i.e., salt-bridges and hydrogen bonds) compared to Mcl-1. However, this general observation provides an example of the limits of a purely static structural analysis of these protein interactions because it offers no basis for specificity differences between Bcl-2 and Mcl-1 and also (incorrectly) suggests that Bcl-2 should bind all BH3 targets tested more tightly than Mcl-1. Nonetheless, the homology modeling approach was able to capture important interactions that were reflected in the HDX data. Specifically, the conserved salt bridge between R146 (Bcl-2) or R263 (Mcl-1) in the BH1 domain at the α4−α5 loop and D_{BH3} (i+9) was detected in all interactions (see Table S5 for BH3 residues). In the case of Bcl-2/Bid, salt-bridge and hydrogen bond interactions were observed at the C-termini of α2 (R107), α3 (L119), α4-α5 loop/5 (N143, R146), and α7 (L201, Y202). For Bcl-2/Bim, interactions were observed at α2 (R107, Y108), α3 (Q118), α4 (R129, E136), and α4−α5 loop/5 (N143, W144, G145, R146), many of which were reflected in the HDX data. For Bcl-2/Bad, there appears to be a restructuring at the α2−α3 region to enable two binding interactions (Y108, D111) in addition to salt bridges at the C- and N-termini of α4 (R129, E136) and α4−α5 loop/5 (R146) and the C-terminus of α7 (E200, G203). These α4 N-terminal and α7 interactions were not detected by HDX. It is not clear if this is a result of a lack of sensitivity of HDX to these particular changes, the presence of a His tag, or an incorrect prediction from the homology modeling approach we are using here.

One unique difference for Mcl-1 interactions predicted by homology modeling, NMR, and crystal structures was that none of the heterodimerizations involved α3. For Mcl-1/Bim (PDB 2PQK), interactions were formed at the α2−α3 loop (H224), as well as the middle and C-terminal region of α4 (R248, H252, V253, N260, and R263). For Mcl-1/Bid (PDB 2KBW), the interaction did not occur at the conserved Arg−Asp salt bridge, but rather with a neighboring residue (N260), as well as a single salt-bridge at the N-terminus of α4 (D242). As for Mcl-1/Noxa, homology modeling revealed interactions at the C-termini of α4 (H252, V253, and S247), α4−α5/α5 (N257, G262, R263), and α7 (F318). An aspect of the experimental data that is supported by the homology models is the observation of an IMS drift-time increase for Bcl-2 and a drift-time decrease for Mcl-1 upon complexation. This is reflected by the fact that in the Bcl-2 models, the BH3 peptide lies "flat" across the binding grove, with little penetration into it. Conversely, in Mcl-1 models, the BH3 peptide is partially enclosed in the binding groove by α3 and α4.

https://doi.org/10.1021/acs.biochem.2c00709
Biochemistry 2023, 62, 1619−1630

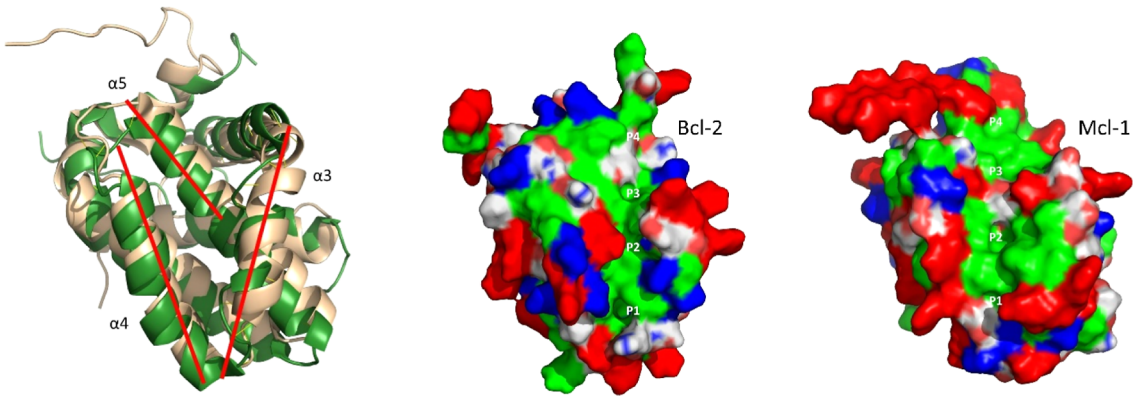

Figure 5. Backbone aligned Mcl-1 and Bcl-2 structure and electrostatics. Left: Mcl-1 (yellow) and Bcl-2 (green) share the Bcl-2 homology core, which includes the conserved BH3 binding groove composed of helices $\alpha3-\alpha5$ (red lines). The solution structures used here were 2MHS (Mcl-1) and 1G5M (Bcl-2).[8,9] Right: Bcl-2 and Mcl-1 color-coded with acidic amino acids in blue, basic amino acids in red, and hydrophobic pockets denoted as P1−P4 in green regions.

DISCUSSION

In this work, we have explored the binding of Mcl-1 and Bcl-2 each to three target and one non-target BH3 peptides with the aim of shedding light on how binding specificity can lead to the formation of protein families with a high degree of structural similarity. To emphasize this structural similarity, a backbone-aligned structural overlay of these proteins is shown in Figure 5. The basis of heterodimerization between pro- and anti-apoptotic family members has long been thought to be driven primarily by hydrophobic interactions.[1] The BH3 groove in anti-apoptotic members is composed of $\alpha3-\alpha5$, which has four hydrophobic "pockets," denoted as P1−P4, and a conserved Arg residue at in the BH1 domain ($\alpha4-\alpha5$ loop).[42] The BH3-only proapoptotic members have a conserved Asp ($i + 9$) and four hydrophobic residues: H1 (i), H2 ($i + 4$), H3 ($i + 7$), and H4 ($i + 11$), which line up to form the hydrophobic face of the amphipathic BH3 helix. The conserved Asp and Arg form an intermolecular salt bridge at the BH1 domain of Bcl-2 and Mcl-1 ($\alpha4-\alpha5$ hinge DGV(T_{Mcl1})NWGR).[43] While these conserved interactions can be used to rationalize the strongly divergent specificity between pro- and anti-apoptotic Bcl-2 proteins, they cannot explain specificity within the anti-apoptotic group of Bcl-2 family proteins like Bcl-2 and Mcl-1, whose specificity profiles are distinct, yet significantly overlapping.

Bcl-2 and Mcl-1 Have Similar Tertiary Folds, but Dissimilar Charge Profiles. The Bcl-2 and Mcl-1 constructs used in this work both consist of 7 α-helices: the predominantly hydrophobic helix $\alpha5$ makes up the core of both proteins, which is surrounded by amphipathic helices $\alpha1-4$ and $\alpha6-7$.[44] Distinctly, the $\alpha3$ in Bcl-2 is considered a 3^{10}-helix. Native MS revealed that despite their different masses, both recombinant Bcl-2 and Mcl-1 exhibit highly similar, narrow, low charge magnitude charge-state envelopes. This suggests that these proteins were ionized with the broadly comparable structural topology that is conserved within the anti-apoptotic Bcl-2 family members and is consistent with their known structures (Figure 5).[8,9,14] A sequence alignment of Bcl-2 and Mcl-1 and their superimposable BH domains is provided in Figure S16, as well as publications where sequence alignment of other Bcl-2 family members and species orthologues can be found.

Gas Phase Measurements Suggest Distinctive Unbound Conformational Ensembles and Divergent Conformational Shifts in Bcl-2 and Mcl-1 upon Complexation. Despite their similarity in NMR structures, IMS data show a distinct difference in drift time between unbound Bcl-2 and Mcl-1, with Mcl-1 exhibiting longer drift times than Bcl-2. This observation is consistent with previous work suggesting that Mcl-1 has a more flexible binding groove than other antiapoptotic members of the Bcl-2 family.[9] The multimodal distributions in the IMS data also point to coexisting conformations in the gas phase that may reflect low-abundance conformational configurations in solution. The presence of these configurations in solution cannot be directly confirmed by global HDX (which is almost always conformationally averaged under "native-like" conditions), but global HDX data nonetheless support the general conclusion that unbound Mcl-1 is more dynamic in solution than unbound Bcl-2 (Figure S6).

When in complex with Bid BH3, the dominant configuration of Mcl-1 exhibits a decreased IMS drift time, which would be consistent with substantial penetration of the BH3 peptide into the binding groove coupled with an overall "tightening" of the protein structure (Figure 2, left column). However, the dominant IMS peak is accompanied by a broad, substantially higher drift time peak, which indicates that a significant fraction of the Mcl-1 population has undergone a conformational shift, making the protein structure more extended and heterogeneous (or more susceptible to unfolding in the gas phase) upon complexation. While the dominant Mcl-1/Bid IMS peak shift is easily rationalized in the context of complexation, it is not clear what binding effects might generate the minor peak corresponding to a less ordered configuration. Conformational disruption associated with binding is technically possible and has been observed previously with myoglobin[45] and lipocalin.[46]

Conversely, Bcl-2 bound to Bid BH3 has a narrowly distributed, longer drift time peak that is indicative of a larger collisional cross section compared to unbound Bcl-2 (Figure 2, right column). This could imply that Bid binding does not involve deep penetration of the BH3 peptide into the Bcl-2 binding groove and does not require substantial rearrangement of the protein structure, which would be consistent with most observations from conventional structural studies[43] and our homology modeling analysis. However, it is as always difficult to draw unambiguous conclusions about processes occurring in solution from IMS data alone, and the appearance of a highly

https://doi.org/10.1021/acs.biochem.2c00709
Biochemistry 2023, 62, 1619−1630

compact minor peak upon binding (Figure 3, bottom right) does not fit with this narrative. Despite the inherent ambiguities in interpreting ion mobility data, the IMS analysis clearly suggests that Mcl-1 and Bcl-2 undergo different conformational transitions when binding the same BH3 peptide.

Bcl-2 and Mcl-1 Undergo Substantially Different Conformational Rearrangements upon Complexation. Differential peptide-level HDX unambiguously showed that Bcl-2 and Mcl-1 each exhibit a unique, protein-specific structural and dynamic behavior during binding, regardless of the BH3 peptide that is bound. Mcl-1 undergoes a large, broadly distributed conformational change within the binding groove at $\alpha3-\alpha5$. To the best of our knowledge, Bcl-2 has never been studied by HDX-MS; however, in agreement with our findings, previously published work by Lee et al. (2016) reported broadly distributed decreases in deuterium uptake for Mcl-1/Bid at a 10 s HDX timepoint.[13] Using LC-HDX-MS, they detected high magnitude decreases at $\alpha3$, $\alpha4$, the C-terminal of $\alpha2$, and the N-terminal of $\alpha5$, which is a more spatially constrained effect than we observe here, likely a result of the improved sensitivity of rapid HDX measurements to subtle changes in dynamics. In contrast to Mcl-1, Bcl-2 exhibits a decrease in uptake that is localized specifically to the $\alpha4-\alpha5$ hinge when in complex with Bim and a small decrease at the C-terminal end of $\alpha3$ for two out of three binders (Bim and Bid).

Comprehensive studies in vitro and in silico have identified critical residues necessary in BH3 binding for Bcl-2 and Mcl-1: F104, Y108, L119, E136, L137, N143, and R146, and V220, V253, N260, R263, and F319, respectively.[27,47−50] For Bcl-2, most of these critical residues are represented in, or nearby, regions of deuterium decrease upon complexation (Figure 3) and salt-bridges/hydrogen bonds observed in homology models (Figure 4). Critical residues F104 and Y108 were not observed because they fall within a peptide region that lacks coverage in Bcl2/Bid and Bcl2/Bad (104−112), and a higher propagated error/variation in Bcl2/Bim and Bcl2/Noxa was observed. An in silico study by Raghav et al. (2012) found that residues 108−135 of Bcl-2 ($\alpha2-\alpha3$ loop, $\alpha3$, and$\alpha3-\alpha4$ loop) are associated with a "large dynamic motion" and that the flexibility of 108−116 ($\alpha2-\alpha3$ loop) may enable the plasticity of the BH3 groove.[51] Peptide 116−130 showed weak HDX differences, but they may have been averaged out across this relatively larger peptide (16 residues), and these changes are further supported by salt-bridges in homology models of Bcl-2/Bid and Bcl-2/Bim.

For Mcl-1, the critical residues all fell within regions experiencing reduced deuterium uptake upon complexation and agreed with the BH3-bound homology model, NMR, and crystal structure. Campbell et al. (2015) have suggested that promiscuous binding is enabled by hotspots that are not conserved between Bcl-2 family members: Mcl-1 has consistent hotspots to enable BH3 binding (V220, N260, R263, and F319), but Bcl-2 hotspots are dispersed across the binding pocket.[47] Although this agrees with the homology models of Bcl-2 and Mcl-1, this critical residue/hotspot model falls short of explaining the decreased deuterium uptake spread across the Mcl-1 BH3 groove and particularly $\alpha3$ where no hotspots existed. However, studies conducted in silico have noted the importance of flexibility in the $\alpha3-\alpha4$ loop of Mcl-1 to enable adjustment of the $\alpha4$ helix.[48,49]

Cumulatively, these studies, along with the HDX and homology modeling data, may support a conformational change in Mcl-1 that occurs within $\alpha3$ to accommodate BH3 peptides, whereas dispersed Bcl-2 hotspots form contacts without the need for extensive conformational adjustment. This is quite contrary to in silico observations that Mcl-1 did not undergo backbone conformational changes to accommodate BH3 peptides whereas Bcl-2 type proteins did.[50]

Overall, our TRESI-HDX data indicate that Mcl-1 must undergo a substantial change in structure and/or dynamics to drive heterodimerization, whereas in Bcl-2, binding is driven less by dynamic shifts and more by specific charge−charge interactions at the BH1/BH3 interface as indicated by homology modeling. A cursory explanation based on this observation could be that higher flexibility in the Mcl-1 binding pocket results in "specificity" simply because it allows for the accommodation of larger BH3 ligands. However, the BH3 ligands used in this study are all similar in size. An alternative explanation arises from a recent study on the N-terminal domain of p53 whose binding specificity is modulated by phosphorylation at specific sites.[52] In that case, the authors demonstrated that conformational instability of the phosphorylated state can be a thermodynamic driver of complexation when the phosphorylated and unphosphorylated bound states had a similar conformational stability. Translated to the current system, this rationale would argue that the higher degree of conformational instability in unbound Mcl-1 (as observed in IMS and global HDX), together with the fact that BH3-bound Mcl-1 and Bcl-2 have similar conformational stabilities, provides a driving force for complexation that is unique to Mcl-1. In such a model, Mcl-1 specificity would arise primarily from the extent to which a "potential binder" BH3 domain is able induce the necessary shift in dynamics upon complexation.

CONCLUSIONS

From the perspective of molecular evolution, these results provide a potential hypothesis as to how the specificity of interactions between proteins can be altered through a difficult-to-predict set of mutations. In recent work, it was demonstrated that the evolution of Mcl-1 and Bcl-2 specificity was "path-dependent", implying that divergent evolutionary pathways generate unique and functionally inequivalent solutions (i.e., sets of mutations) to subsequent evolutionary challenges.[53] The results of the current work reinforce the view that specificity is not always dictated by specific amino acid substitutions at the interface but can also be driven by widely dispersed mutations that impact protein-wide conformational dynamics. Future efforts examining how alterations in protein dynamics impacted the evolution of functions within Mcl-1 and Bcl-2 orthologues, and specifically whether there is an identifiable "branch-point" ancestor whose evolution diverged into "charge-dominated" and "dynamics dominated" branches, could shed light on how native protein functions emerged, and could also provide new approaches for engineering novel binding specificity profiles into biomolecules.

From the perspective of practical outcomes from this type of analysis, a more complete understanding of binding specificity among structurally similar proteins is a foundation for the development of targeted therapeutics in many "challenging" protein families, including the Bcl-2, GST, LXR, and GPCR families among many others. Our hope is that further explorations of the dynamic drivers of binding specificity will encourage drug development targeting not just structures but function-critical dynamic transitions.

https://doi.org/10.1021/acs.biochem.2c00709
Biochemistry 2023, 62, 1619−1630

■ ASSOCIATED CONTENT

Supporting Information

The Supporting Information is available free of charge at https://pubs.acs.org/doi/10.1021/acs.biochem.2c00709.

Cell-based assays demonstrating Bcl-2 and Mcl-1 construct function, Bcl-2 and Mcl-1 construct sequence information, sequence coverage and peptide lists for HDX-MS experiments, additional ion mobility data for different charge states, global HDX of Bcl-2 and Mcl-1, and raw deuterium uptake kinetics plots (PDF)

Accession Codes

Mcl-1 Uniprot: Q07820 https://www.uniprot.org/uniprotkb/Q07820/entry. Bcl-2 Uniprot: P10415 https://www.uniprot.org/uniprotkb/P10415/entry

■ AUTHOR INFORMATION

Corresponding Author

Derek J. Wilson − *Department of Chemistry, York University, Toronto, Ontario M3J 1P3, Canada;* orcid.org/0000-0002-7012-6085; Phone: (416) 736-2100; Email: dkwilson@yorku.ca

Authors

Esther Wolf − *Department of Chemistry, York University, Toronto, Ontario M3J 1P3, Canada*

Cristina Lento − *Department of Chemistry, York University, Toronto, Ontario M3J 1P3, Canada*

Jinyue Pu − *Department of Chemistry, University of Chicago, Chicago, Illinois 60637, United States*

Bryan C. Dickinson − *Department of Chemistry, University of Chicago, Chicago, Illinois 60637, United States;* orcid.org/0000-0002-9616-1911

Complete contact information is available at: https://pubs.acs.org/10.1021/acs.biochem.2c00709

Author Contributions

E.W. and D.J.W. contributed equally to writing the manuscript, E.W. and J.P. performed experiments, and D.J.W., C.L., and B.C.D. provided supervision. All authors have given their approval to the final version of the manuscript.

Notes

The authors declare no competing financial interest.

■ ACKNOWLEDGMENTS

This work was supported by the Natural Sciences and Engineering Research Council (NSERC) of Canada Collaborative Research and Development (CRD) (CRDPJ 485321-15) Program, the Discovery Program (RGPIN 480432), and the National Institute of General Medical Sciences (R35 GM119840) of the National Institutes of Health (B.C.D.).

■ ABBREVIATIONS

Bcl-2	B-cell lymphoma 2 protein
BH	Bcl-2 homology domain
ESI-MS	electrospray ionization mass spectrometry
HDX-MS	hydrogen−deuterium exchange mass spectrometry
IMS	ion mobility spectrometry
Mcl-1	Induced myeloid leukemia cell differentiation protein
MOMP	mitochondrial outer membrane permeabilization
PDB	protein data bank
rmsd	root mean squared deviation
tBid	truncated Bid
TRESI	time-resolved electrospray ionoization

■ REFERENCES

(1) Kale, J.; Osterlund, E. J.; Andrews, D. W. BCL-2 Family Proteins: Changing Partners in the Dance towards Death. *Cell Death Differ.* **2018**, *25*, 65−80.

(2) Luo, X.; Budihardjo, I.; Zou, H.; Slaughter, C.; Wang, X. Bid, a Bcl2 Interacting Protein, Mediates Cytochrome c Release from Mitochondria in Response to Activation of Cell Surface Death Receptors. *Cell* **1998**, *94*, 481−490.

(3) Westphal, D.; Kluck, R. M.; Dewson, G. Building Blocks of the Apoptotic Pore: How Bax and Bak Are Activated and Oligomerize during Apoptosis. *Cell Death Differ.* **2014**, *21*, 196−205.

(4) Baliga, B.; Kumar, S. Apaf-1/Cytochrome c Apoptosome: An Essential Initiatorof Caspase Activation or Just a Sideshow? *Cell Death Differ.* **2003**, *10*, 16−18.

(5) Altschul, S. F.; Wootton, J. C.; Gertz, E. M.; Agarwala, R.; Morgulis, A.; Schäffer, A. A.; Yu, Y.-K. Protein Database Searches Using Compositionally Adjusted Substitution Matrices. *FEBS J.* **2005**, *272*, 5101−5109.

(6) Altschul, S. F.; Madden, T. L.; Schäffer, A. A.; Zhang, J.; Zhang, Z.; Miller, W.; Lipman, D. J. Gapped BLAST and PSI-BLAST: A New Generation of Protein Database Search Programs. *Nucleic Acids Res.* **1997**, *25*, 3389−3402.

(7) Schrödinger, L. L. C. *The PyMOL Molecular Graphics System.* Version 1.8, 2015;.

(8) Petros, A. M.; Medek, A.; Nettesheim, D. G.; Kim, D. H.; Yoon, H. S.; Swift, K.; Matayoshi, E. D.; Oltersdorf, T.; Fesik, S. W. Solution Structure of the Antiapoptotic Protein Bcl-2. *Proc. Natl. Acad. Sci. U.S.A.* **2001**, *98*, 3012−3017.

(9) Liu, G.; Poppe, L.; Aoki, K.; Yamane, H.; Lewis, J.; Szyperski, T. High-Quality NMR Structure of Human Anti-Apoptotic Protein Domain Mcl-1(171-327) for Cancer Drug Design. *PLoS One* **2014**, *9*, No. e96521.

(10) Liu, X. R.; Zhang, M. M.; Gross, M. L. Mass Spectrometry-Based Protein Footprinting for Higher-Order Structure Analysis: Fundamentals and Applications. *Chem. Rev.* **2020**, *120*, 4355−4454.

(11) Rob, T.; Liuni, P.; Gill, P. K.; Zhu, S.; Balachandran, N.; Berti, P. J.; Wilson, D. J. Measuring Dynamics in Weakly Structured Regions of Proteins Using Microfluidics-Enabled Subsecond H/D Exchange Mass Spectrometry. *Anal. Chem.* **2012**, *84*, 3771−3779.

(12) Lento, C.; Wilson, D. J. Subsecond Time-Resolved Mass Spectrometry in Dynamic Structural Biology. *Chem. Rev.* **2022**, *122*, 7624−7646.

(13) Lee, S.; Wales, T. E.; Escudero, S.; Cohen, D. T.; Luccarelli, J.; Gallagher, C. G.; Cohen, N. A.; Huhn, A. J.; Bird, G. H.; Engen, J. R.; Walensky, L. D. Allosteric Inhibition of Antiapoptotic MCL-1. *Nat. Struct. Mol. Biol.* **2016**, *23*, 600−607.

(14) Day, C. L.; Chen, L.; Richardson, S. J.; Harrison, P. J.; Huang, D. C. S.; Hinds, M. G. Solution Structure of Prosurvival Mcl-1 and Characterization of Its Binding by Proapoptotic BH3-Only Ligands. *J. Biol. Chem.* **2005**, *280*, 4738−4744.

(15) Wilson, D. J.; Konermann, L. A Capillary Mixer with Adjustable Reaction Chamber Volume for Millisecond Time-Resolved Studies by Electrospray Mass Spectrometry. *Anal. Chem.* **2003**, *75*, 6408−6414.

(16) Lento, C.; Zhu, S.; Brown, K. A.; Knox, R.; Liuni, P.; Wilson, D. J. Time-Resolved ElectroSpray Ionization Hydrogen-Deuterium Exchange Mass Spectrometry for Studying Protein Structure and Dynamics. *J. Vis. Exp.* **2017**, *122*, No. e55464.

(17) Rey, M.; Sarpe, V.; Burns, K. M.; Buse, J.; Baker, C. A. H.; van Dijk, M.; Wordeman, L.; Bonvin, A. M. J. J.; Schriemer, D. C. Mass Spec Studio for Integrative Structural Biology. *Structure* **2014**, *22*, 1538−1548.

(18) Gattiker, A.; Bienvenut, W. V.; Bairoch, A.; Gasteiger, E. FindPept, a Tool to Identify Unmatched Masses in Peptide Mass Fingerprinting Protein Identification. *Proteomics* **2002**, *2*, 1435−1444.

(19) Waterhouse, A.; Bertoni, M.; Bienert, S.; Studer, G.; Tauriello, G.; Gumienny, R.; Heer, F. T.; de Beer, T. A.; Rempfer, C.; Bordoli, L.; Lepore, R.; Schwede, T. SWISS-MODEL: Homology Modelling of Protein Structures and Complexes. *Nucleic Acids Res.* **2018**, *46*, W296−W303.
(20) Studer, G.; Rempfer, C.; Waterhouse, A. M.; Gumienny, R.; Haas, J.; Schwede, T. QMEANDisCo—Distance Constraints Applied on Model Quality Estimation. *Bioinformatics* **2020**, *36*, 1765−1771.
(21) Sattler, M.; Liang, H.; Nettesheim, D.; Meadows, R. P.; Harlan, J. E.; Eberstadt, M.; Yoon, H. S.; Shuker, S. B.; Chang, B. S.; Minn, A. J.; Thompson, C. B.; Fesik, S. W. Structure of Bcl-XL-Bak Peptide Complex: Recognition Between Regulators of Apoptosis. *Science* **1997**, *275*, 983−986.
(22) Pu, J.; Dewey, J. A.; Hadji, A.; LaBelle, J. L.; Dickinson, B. C. RNA Polymerase Tags To Monitor Multidimensional Protein−Protein Interactions Reveal Pharmacological Engagement of Bcl-2 Proteins. *J. Am. Chem. Soc.* **2017**, *139*, 11964−11972.
(23) Carlson, J. C.; Badran, A. H.; Guggiana-Nilo, D. A.; Liu, D. R. Negative Selection and Stringency Modulation in Phage-Assisted Continuous Evolution. *Nat. Chem. Biol.* **2014**, *10*, 216−222.
(24) Certo, M.; Moore, V. D. G.; Nishino, M.; Wei, G.; Korsmeyer, S.; Armstrong, S. A.; Letai, A. Mitochondria Primed by Death Signals Determine Cellular Addiction to Antiapoptotic BCL-2 Family Members. *Cancer Cell* **2006**, *9*, 351−365.
(25) Letai, A.; Bassik, M. C.; Walensky, L. D.; Sorcinelli, M. D.; Weiler, S.; Korsmeyer, S. J. Distinct BH3 Domains Either Sensitize or Activate Mitochondrial Apoptosis, Serving as Prototype Cancer Therapeutics. *Cancer Cell* **2002**, *2*, 183−192.
(26) Smith, A. J.; Dai, H.; Correia, C.; Takahashi, R.; Lee, S.-H.; Schmitz, I.; Kaufmann, S. H. Noxa/Bcl-2 Protein Interactions Contribute to Bortezomib Resistance in Human Lymphoid Cells. *J. Biol. Chem.* **2011**, *286*, 17682−17692.
(27) Chen, L.; Willis, S. N.; Wei, A.; Smith, B. J.; Fletcher, J. I.; Hinds, M. G.; Colman, P. M.; Day, C. L.; Adams, J. M.; Huang, D. C. S. Differential Targeting of Prosurvival Bcl-2 Proteins by Their BH3-Only Ligands Allows Complementary Apoptotic Function. *Mol. Cell* **2005**, *17*, 393−403.
(28) Dai, H.; Pang, Y.-P.; Ramirez-Alvarado, M.; Kaufmann, S. H. Evaluation of the BH3-Only Protein Puma as a Direct Bak Activator. *J. Biol. Chem.* **2014**, *289*, 89−99.
(29) Du, Y.; Nikolovska-Coleska, Z.; Qui, M.; Li, L.; Lewis, I.; Dingledine, R.; Stuckey, J. A.; Krajewski, K.; Roller, P. P.; Wang, S.; Fu, H. A Dual-Readout F2 Assay That Combines Fluorescence Resonance Energy Transfer and Fluorescence Polarization for Monitoring Bimolecular Interactions. *Assay Drug Dev. Technol.* **2011**, *9*, 382−393.
(30) Liu, Q.; Moldoveanu, T.; Sprules, T.; Matta-Camacho, E.; Mansur-Azzam, N.; Gehring, K. Apoptotic Regulation by MCL-1 through Heterodimerization. *J. Biol. Chem.* **2010**, *285*, 19615−19624.
(31) Bhat, V.; Olenick, M. B.; Schuchardt, B. J.; Mikles, D. C.; McDonald, C. B.; Farooq, A. Biophysical Basis of the Promiscuous Binding of B-Cell Lymphoma Protein 2 Apoptotic Repressor to BH3 Ligands. *J. Mol. Recognit.* **2013**, *26*, 501−513.
(32) Ku, B.; Liang, C.; Jung, J. U.; Oh, B.-H. Evidence That Inhibition of BAX Activation by BCL-2 Involves Its Tight and Preferential Interaction with the BH3 Domain of BAX. *Cell Res.* **2011**, *21*, 627−641.
(33) Day, C. L.; Smits, C.; Fan, F. C.; Lee, E. F.; Fairlie, W. D.; Hinds, M. G. Structure of the BH3 Domains from the P53-Inducible BH3-Only Proteins Noxa and Puma in Complex with Mcl-1. *J. Mol. Biol.* **2008**, *380*, 958−971.
(34) Czabotar, P. E.; Lee, E. F.; van Delft, M. F.; Day, C. L.; Smith, B. J.; Huang, D. C. S.; Fairlie, W. D.; Hinds, M. G.; Colman, P. M. Structural Insights into the Degradation of Mcl-1 Induced by BH3 Domains. *Proc. Natl. Acad. Sci. U.S.A* **2007**, *104*, 6217−6222.
(35) Anasir, M. I.; Caria, S.; Skinner, M. A.; Kvansakul, M. Structural Basis of Apoptosis Inhibition by the Fowlpox Virus Protein FPV039. *J. Biol. Chem.* **2017**, *292*, 9010−9021.
(36) Dutta, S.; Chen, T. S.; Keating, A. E. Peptide Ligands for Pro-Survival Protein Bfl-1 from Computationally Guided Library Screening. *ACS Chem. Biol.* **2013**, *8*, 778−788.
(37) Foight, G. W.; Ryan, J. A.; Gullá, S. V.; Letai, A.; Keating, A. E. Designed BH3 Peptides with High Affinity and Specificity for Targeting Mcl-1 in Cells. *ACS Chem. Biol.* **2014**, *9*, 1962−1968.
(38) Winkler, R. ESIprot: a universal tool for charge state determination and molecular weight calculation of proteins from electrospray ionization mass spectrometry data: ESIprot: a universal tool for the analysis of protein ESI-MS data. *Rapid Commun. Mass Spectrom.* **2010**, *24*, 285−294.
(39) Kitova, E. N.; El-Hawiet, A.; Schnier, P. D.; Klassen, J. S. Reliable Determinations of Protein−Ligand Interactions by Direct ESI-MS Measurements. Are We There Yet? *J. Am. Soc. Mass Spectrom.* **2012**, *23*, 431−441.
(40) Macias, L. A.; Santos, I. C.; Brodbelt, J. S. Ion Activation Methods for Peptides and Proteins. *Anal. Chem.* **2020**, *92*, 227−251.
(41) Konermann, L.; Ahadi, E.; Rodriguez, A. D.; Vahidi, S. Unraveling the Mechanism of Electrospray Ionization. *Anal. Chem.* **2013**, *85*, 2−9.
(42) Denis, C.; Sopková-de Oliveira Santos, J.; Bureau, R.; Voisin-Chiret, A. S. Hot-Spots of Mcl-1 Protein. *J. Med. Chem.* **2020**, *63*, 928−943.
(43) Petros, A. M.; Olejniczak, E. T.; Fesik, S. W. Structural Biology of the Bcl-2 Family of Proteins. *Biochim. Biophys. Acta, Mol. Cell Res.* **2004**, *1644*, 83−94.
(44) Banjara, S.; Suraweera, C. D.; Hinds, M. G.; Kvansakul, M. The Bcl-2 Family: Ancient Origins, Conserved Structures, and Divergent Mechanisms. *Biomolecules* **2020**, *10*, 128.
(45) Konermann, L.; Rodriguez, A. D.; Sowole, M. A. Type 1 and Type 2 Scenarios in Hydrogen Exchange Mass Spectrometry Studies on Protein−Ligand Complexes. *Analyst* **2014**, *139*, 6078−6087.
(46) Huang, X.; Slavkovic, S.; Song, E.; Botta, A.; Mehrazma, B.; Lento, C.; Johnson, P. E.; Sweeney, G.; Wilson, D. J. A Unique Conformational Distortion Mechanism Drives Lipocalin 2 Binding to Bacterial Siderophores. *ACS Chem. Biol.* **2020**, *15*, 234−242.
(47) Campbell, S. T.; Carlson, K. J.; Buchholz, C. J.; Helmers, M. R.; Ghosh, I. Mapping the BH3 Binding Interface of Bcl-XL, Bcl-2, and Mcl-1 Using Split-Luciferase Reassembly. *Biochemistry* **2015**, *54*, 2632−2643.
(48) Zhao, R.-N.; Fan, S.; Han, J.-G.; Liu, G. Molecular Dynamics Study of Segment Peptides of Bax, Bim, and Mcl-1 BH3 Domain of the Apoptosis-Regulating Proteins Bound to the Anti-Apoptotic Mcl-1 Protein. *J. Biomol. Struct. Dyn.* **2015**, *33*, 1067−1081.
(49) Fogha, J.; Marekha, B.; De Giorgi, M.; Voisin-Chiret, A. S.; Rault, S.; Bureau, R.; Sopkova-de Oliveira Santos, J. Toward Understanding Mcl-1 Promiscuous and Specific Binding Mode. *J. Chem. Inf. Model.* **2017**, *57*, 2885−2895.
(50) Ivanov, S. M.; Huber, R. G.; Warwicker, J.; Bond, P. J. Energetics and Dynamics Across the Bcl-2-Regulated Apoptotic Pathway Reveal Distinct Evolutionary Determinants of Specificity and Affinity. *Structure* **2016**, *24*, 2024−2033.
(51) Raghav, P. K.; Verma, Y. K.; Gangenahalli, G. U. Molecular Dynamics Simulations of the Bcl-2 Protein to Predict the Structure of Its Unordered Flexible Loop Domain. *J. Mol. Model.* **2012**, *18*, 1885−1906.
(52) Zhu, S.; Khatun, R.; Lento, C.; Sheng, Y.; Wilson, D. J. Enhanced Binding Affinity via Destabilization of the Unbound State: A Millisecond Hydrogen−Deuterium Exchange Study of the Interaction between P53 and a Pleckstrin Homology Domain. *Biochemistry* **2017**, *56*, 4127−4133.
(53) Xie, V. C.; Pu, J.; Metzger, B. P.; Thornton, J. W.; Dickinson, B. C. Contingency and Chance Erase Necessity in the Experimental Evolution of Ancestral Proteins. *eLife* **2021**, *10*, No. e67336.

https://doi.org/10.1021/acs.biochem.2c00709
Biochemistry 2023, 62, 1619−1630